Geometric Tricopter Controller

Tomasz Frelek
University of California San Diego
San Diego, USA
tfrelek@ucsd.edu

***Abstract*—This paper presents a geometric tracking control strategy for a standard tricopter unmanned aerial vehicle (UAV). Unlike quadrotors, the tricopter utilizes a tilting rear rotor for yaw control, introducing a nonlinear coupling between the heading moment and lateral translational dynamics. We develop a nonlinear control allocation scheme that resolves this coupling, allowing the attitude dynamics to be treated as a fully actuated rigid body while isolating the parasitic lateral forces as bounded disturbances. The control law is defined globally on the special Euclidean group $SE(3)$, avoiding singularities associated with Euler angles and ambiguities inherent to quaternions. We provide a rigorous Lyapunov stability analysis demonstrating that the attitude tracking errors converge exponentially to zero, while the translational tracking errors are Uniformly Ultimately Bounded (UUB). Furthermore, the controller is shown to exhibit almost global attractiveness, ensuring recovery from large initial attitude errors. The proposed framework provides a robust solution for complex, large-angle maneuvers where linear control methods typically fail.**

I. INTRODUCTION

A tricopter unmanned aerial vehicle (UAV) consists of three rotors located at the vertices of a triangular frame, typically in a T or Y-configuration. Unlike the quadrotor, which relies on four fixed counter-rotating propellers, the standard tricopter utilizes two fixed front rotors and a single rear rotor mounted on a tilting servo mechanism. This configuration provides distinct agility advantages, particularly in yaw authority, as the heading is controlled by the vectoring of the rear thrust rather than the relatively weak differential drag torque used in quadrotors. Due to this mechanical structure, tricopters have been envisaged for applications requiring high maneuverability and have become a popular platform for both research and hobbyist communities.

Despite the unique characteristics of tricopter UAVs, the development of nonlinear control systems for them has often lagged behind that of quadrotors. Common approaches rely on linear control systems such as proportional-derivative (PD) controllers or linear quadratic regulators (LQR) applied to linearized dynamics. While effective for near-hover conditions, these approaches fundamentally restrict the vehicle's ability to perform complex, large-angle maneuvers. Furthermore, nonlinear controllers based on Euler angles exhibit singularities when representing complex rotational maneuvers, limiting the flight envelope and potentially leading to control failure at critical attitudes. To overcome these limitations, we turn to control methods defined directly on the configuration manifold.

Geometric control is concerned with the development of control systems for dynamic systems evolving on nonlinear manifolds that cannot be globally identified with Euclidean spaces. By characterizing geometric properties of nonlinear manifolds intrinsically, geometric control techniques provide unique insights to control theory that cannot be obtained from dynamic models represented using local coordinates. This approach has been successfully applied to fully actuated rigid body dynamics on Lie groups [1], [2], and to underactuated quadrotor UAVs to achieve almost global asymptotic stability on the special Euclidean group $SE(3)$ [3], [4]. However, these formulations are inapplicable to the proposed tricopter configuration due to the mechanical coupling between yaw and lateral translation. Unlike standard quadrotor models which assume a net thrust vector strictly fixed along the body z-axis, the tricopter's tilting tail mechanism introduces a servo-dependent lateral force component that violates the underactuated input assumptions inherent in standard $SE(3)$ geometric tracking controls.

While there has been work done developing geometric controllers for other tricopter layouts [5], to our knowledge there has not been a geometric controller developed specifically for the most common tricopter layout: a Y shape with two equidistant fixed-frame forward rotors offset at the same angle, and a rear tilt rotor as show in 1.

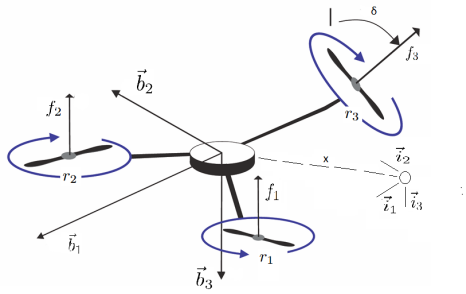

Fig. 1. Model Tricopter

In this paper, we develop a geometric controller for a standard tricopter UAV. The dynamics of the tricopter are expressed globally on the configuration manifold of $SE(3)$. We construct a tracking controller to follow prescribed trajectories for the center of mass and heading direction. However, distinct from the quadrotor case, the tricopter introduces a unique coupling between the yaw moment and the lateral translational dynamics. The tilting of the rear rotor, required for yaw control, generates a parasitic lateral force that prevents the thrust vector from remaining strictly body-fixed. We derive

a nonlinear control allocation scheme to address this coupling and show that the resulting closed-loop system exhibits uniformly ultimately bounded (UUB) stability in the presence of these parasitic forces.

Compared to existing geometric control approaches, this work is distinct in that it addresses the specific topological and mechanical constraints of this tricopter format. While the vehicle remains underactuated by controlling six degrees of freedom with four inputs (three motor thrusts and one servo angle), the non-fixed nature of the rear thrust vector requires a modification of the stability analysis. We demonstrate that this controller is capable of stabilizing the tricopter through complex maneuvers, treating the coupling effects as bounded disturbances within the geometric framework.

II. TRICOPTER DYNAMICS MODEL

Consider a tricopter vehicle model illustrated in 1. This system consists of two front rotors fixed to the body frame and one rear rotor mounted on a servo mechanism that allows for tilting in the lateral plane.

We choose an inertial reference frame $\{\vec{i}_1, \vec{i}_2, \vec{i}_3\}$ and a body-fixed frame $\{\vec{b}_1, \vec{b}_2, \vec{b}_3\}$. The origin of the body-fixed frame is located at the center of mass of the vehicle. The first axis $\vec{b}_1$ points forward, the second axis $\vec{b}_2$ points to the right, and the third axis $\vec{b}_3$ points downward.

Define

- $m \in \mathbb{R}$ the total mass
- $x \in \mathbb{R}^3$ the location of the center of mass in the inertial frame
- $J \in \mathbb{R}^{3\times3}$ the inertia matrix with respect to the body-fixed frame
- $R \in SO(3)$ the rotation matrix from the body-fixed frame to the inertial frame
- $\Omega \in \mathbb{R}^3$ the angular velocity in the body-fixed frame
- $d_x, d_y \in \mathbb{R}$ the longitudinal and lateral distance from the center of mass to the front rotors
- $d_t \in \mathbb{R}$ the distance from the center of mass to the rear rotor
- $f_i \in \mathbb{R}$ the thrust generated by the i-th propeller, for $i = \{1, 2, 3\}$
- $\delta \in \mathbb{R}$ the tilt angle of the rear servo, where $\delta > 0$ creates a thrust component in the $+\vec{b}_2$ direction
- $f \in \mathbb{R}$ the total vertical thrust magnitude
- $M \in \mathbb{R}^3$ the total moment in the body-fixed frame

We assume that the thrust of each propeller f_i is directly controlled. The locations of the three rotors in the body frame are given by $r_1 = [d_x; d_y; 0]$, $r_2 = [d_x; -d_y; 0]$, and $r_3 = [-d_t; 0; 0]$.

Under these definitions, the total force vector $F_b \in \mathbb{R}^3$ and the total moment $M \in \mathbb{R}^3$ in the body frame are given by the nonlinear mapping:

$$F_b = \begin{bmatrix} 0 \\ f_3 \sin\delta \\ -(f_1 + f_2 + f_3\cos\delta) \end{bmatrix} \tag{1}$$

$$M = \begin{bmatrix} d_y(f_1 - f_2) \\ -d_x(f_1 + f_2) + d_t f_3 \cos\delta \\ -d_t f_3 \sin\delta \end{bmatrix} \tag{2}$$

To facilitate control design, we define intermediate virtual inputs $f_{3,vert} = f_3\cos\delta$ and $f_{3,lat} = f_3\sin\delta$. This transformation decouples the system, allowing the relationship between the desired virtual controls $\nu_d = [f_d, M_{1d}, M_{2d}, M_{3d}]^T$ and the intermediate actuators $u_{virtual} = [f_1, f_2, f_{3,vert}, f_{3,lat}]^T$ to be expressed as a linear map:

$$\begin{bmatrix} f_d \\ M_{1d} \\ M_{2d} \\ M_{3d} \end{bmatrix} = \begin{bmatrix} 1 & 1 & 1 & 0 \\ d_y & -d_y & 0 & 0 \\ -d_x & -d_x & d_t & 0 \\ 0 & 0 & 0 & -d_t \end{bmatrix} \begin{bmatrix} f_1 \\ f_2 \\ f_{3,vert} \\ f_{3,lat} \end{bmatrix} \tag{3}$$

The equations of motion of this tricopter UAV can be written:

$$\dot{x} = v \tag{4}$$

$$m\dot{v} = mge_3 + RF_b \tag{5}$$

$$\dot{R} = R\hat{\Omega} \tag{6}$$

$$J\dot{\Omega} + \Omega \times J\Omega = M \tag{7}$$

where $e_3 = [0; 0; 1] \in \mathbb{R}^3$. Note that in (5), the term RF_b captures the parasitic lateral forces induced by the vectoring of the rear motor, defined as $\Delta = f_3 \sin\delta \vec{b}_2$.

Note that the configuration of this tricopter UAV is defined by the location of the center of mass and the attitude with respect to the inertial frame. Therefore, the configuration manifold is the special Euclidean group $SE(3)$, which is the semidirect product of $\mathbb{R}^3$ and the special orthogonal group $SO(3) = \{R \in \mathbb{R}^{3\times3} | R^T R = I, \det R = 1\}$.

A. Configuration Manifold Geometry

The configuration space of the tricopter is identified with the Special Euclidean group $SE(3)$ because the vehicle is modeled as a rigid body capable of arbitrary translation and rotation in three-dimensional space.

Mathematically, the group structure is defined as the semi-direct product of the translation group $\mathbb{R}^3$ and the rotation group $SO(3)$, denoted as $SE(3) \cong \mathbb{R}^3 \rtimes SO(3)$. An element $g \in SE(3)$ is represented by the pair (x, R), where $x \in \mathbb{R}^3$ denotes the position of the center of mass in the inertial frame, and $R \in SO(3)$ represents the orientation of the body-fixed frame relative to the inertial frame.

The semi-direct nature of this product defines the group operation (composition of rigid motions). For two configurations $g_1 = (x_1, R_1)$ and $g_2 = (x_2, R_2)$, the group multiplication is given by:

$$g_1 \cdot g_2 = (x_1 + R_1 x_2, R_1 R_2) \tag{8}$$

This operation captures the coupling between rotation and translation: a translation in the body frame (x_2) must be rotated by the current attitude (R_1) to be correctly expressed in the

inertial frame. This structure is often visualized using homogeneous transformation matrices, where an element $g \in SE(3)$ is identified with the matrix:

$$H = \begin{bmatrix} R & x \\ 0_{1\times 3} & 1 \end{bmatrix} \in \mathbb{R}^{4\times 4} \tag{9}$$

In this matrix representation, the group dynamics evolve on the tangent bundle $TSE(3)$. The velocity of the vehicle is defined by the pair (v, Ω), where $v \in \mathbb{R}^3$ is the linear velocity in the inertial frame and $\Omega \in \mathbb{R}^3$ is the angular velocity in the body frame.

III. GEOMETRIC TRACKING CONTROL ON SE(3)

The proposed control architecture is designed to track a reference trajectory defined by a desired center of mass position, $x_d(t)$, and a desired heading direction, $\vec{b}_{1_d}(t)$.

The control design separates the system into translational and rotational subsystems. For the high-level controller, we treat the total vertical thrust magnitude f and the body-frame moment vector M as virtual control inputs. To track the position trajectory $x_d(t)$, the translational controller calculates the required magnitude f and the required direction of the body-fixed vertical axis, denoted as $\vec{b}_{3_d}$.

Constructing the full desired attitude $R_d \in SO(3)$ requires resolving the ambiguity in rotation about this vertical axis. The desired heading vector $\vec{b}_{1_d}(t)$ provides this constraint. Assuming $\vec{b}_{1_d}$ is not collinear with the thrust vector $\vec{b}_{3_d}$, we project the heading onto the plane orthogonal to $\vec{b}_{3_d}$. This yields the intermediate axis $\vec{b}_{2_d} = (\vec{b}_{3_d} \times \vec{b}_{1_d})/||\vec{b}_{3_d} \times \vec{b}_{1_d}||$. The complete rotation matrix is then assembled as $R_d = [\vec{b}_{2_d} \times \vec{b}_{3_d}, \vec{b}_{2_d}, \vec{b}_{3_d}]$. The rotational controller then computes the virtual moment M required to track this R_d.

In summary, the controller computes four virtual inputs to stabilize three translational degrees of freedom and one heading degree of freedom, ensuring $x(t) \to x_d(t)$ and that the projection of the body axis aligns with the desired heading. These virtual commands are subsequently mapped to the physical tricopter actuators (f_1, f_2, f_3, δ) via the nonlinear allocation scheme detailed in Section II.

By formulating the control law directly on the Special Euclidean group $SE(3)$, we avoid the singularities associated with local parametrizations such as Euler angles. This geometric approach ensures the controller remains valid even during complex, large-angle maneuvers.

A. Tracking Errors

The translational tracking errors are defined in the inertial frame as the difference between the actual and desired states:

$$e_x = x - x_d \tag{10}$$

$$e_v = v - v_d \tag{11}$$

where $x_d(t)$ and $v_d(t)$ are the reference position and velocity, respectively.

Defining error metrics on the nonlinear manifold $SO(3)$ requires a more intrinsic approach. We utilize the following configuration error function Ψ, which quantifies the "distance" between the current attitude R and the desired attitude R_d:

$$\Psi(R, R_d) = \frac{1}{2}\mathrm{tr}[I - R_d^T R] \tag{12}$$

This function is locally positive-definite for all rotations where the angular deviation between R and R_d is less than $180°$. Consequently, the sublevel set $L_2 = \{(R_d, R) \in SO(3) \times SO(3) \mid \Psi(R, R_d) < 2\}$ defines a region of attraction that covers almost the entire rotation group.

To derive the attitude error vector, we examine the derivative of Ψ with respect to a variation $\delta R = R\hat{\eta}$, where $\eta \in \mathbb{R}^3$. Utilizing the trace identity $-\frac{1}{2}\mathrm{tr}[\hat{x}\hat{y}] = x^T y$, the derivative can be expressed as:

$$\mathbf{D}_R\Psi(R, R_d) \cdot R\hat{\eta} = \frac{1}{2}(R_d^T R - R^T R_d)^\vee \cdot \eta \tag{13}$$

where $(\cdot)^\vee$ denotes the inverse of the hat map, mapping $\mathfrak{so}(3)$ elements back to $\mathbb{R}^3$. This identifies the attitude tracking error vector e_R as:

$$e_R = \frac{1}{2}(R_d^T R - R^T R_d)^\vee \tag{14}$$

For angular velocity, a direct subtraction is invalid because the velocities $\dot{R}$ and $\dot{R}_d$ reside in different tangent spaces. To define a meaningful error, we transport the desired velocity into the current body frame. The difference between the actual body rate Ω and the desired rate represented in the body frame is given by:

$$e_\Omega = \Omega - R^T R_d \Omega_d \tag{15}$$

Physically, e_Ω corresponds to the angular velocity of the relative rotation matrix $R_d^T R$, verifying that it correctly captures the rotational rate error in the body-fixed frame.

B. Tracking Controller

Given the smooth reference trajectories for position $x_d(t)$ and heading $\vec{b}_{1_d}(t)$, the control design first computes the ideal orientation of the vehicle's vertical axis. By augmenting the position error feedback with the feedforward acceleration term, we define the desired direction of the third body-fixed axis $\vec{b}_{3_d}$ as:

$$\vec{b}_{3_d} = -\frac{-k_x e_x - k_v e_v - mge_3 + m\ddot{x}_d}{||-k_x e_x - k_v e_v - mge_3 + m\ddot{x}_d||} \tag{16}$$

This formulation assumes the denominator remains non-zero, ensuring a well-defined thrust direction. To fully constrain the vehicle's orientation, we utilize the reference heading $\vec{b}_{1_d}$, assuming it is not collinear with $\vec{b}_{3_d}$. The complete desired rotation matrix $R_d \in SO(3)$ is constructed by projecting the heading onto the plane orthogonal to the thrust vector: $R_d = [\vec{b}_{2_d} \times \vec{b}_{3_d}, \vec{b}_{2_d}, \vec{b}_{3_d}]$, utilizing the intermediate vector $\vec{b}_{2_d} = (\vec{b}_{3_d} \times \vec{b}_{1_d})/||\vec{b}_{3_d} \times \vec{b}_{1_d}||$. We further assume the trajectory is feasible such that the required vertical force is bounded, i.e., $||-mge_3 + m\ddot{x}_d|| < B$.

With the desired attitude established, the virtual control inputs—comprising the scalar thrust magnitude f and the

vector moment M—are synthesized to exponentially stabilize the tracking errors:

$$f = -(-k_x e_x - k_v e_v - mge_3 + m\ddot{x}_d) \cdot Re_3 \tag{17}$$

$$M = -k_R e_R - k_\Omega e_\Omega + \Omega \times J\Omega - J(\hat{\Omega} R^T R_d \Omega_d - R^T R_d \dot{\Omega}_d) \tag{18}$$

Here, k_x, k_v, k_R, k_Ω serve as positive control gains.

The final stage of the control architecture maps the computed virtual vector $\nu_d = [f, M_1, M_2, M_3]^T$ to the tricopter's specific actuator configuration. We employ the linear allocation model A_{new} defined in (3). Provided the geometric parameters d_t and d_y are non-zero, the matrix is invertible ($\det(A_{new}) = -2d_y d_t(d_x + d_t)$), allowing us to solve for the intermediate virtual inputs $u_{virtual} = [f_1, f_2, f_{3,vert}, f_{3,lat}]^T$:

$$f_{3,vert} = \frac{M_2 + d_x f}{d_t + d_x}, \quad f_{3,lat} = -\frac{M_3}{d_t} \tag{19}$$

These Cartesian components are then converted into the physical commands for the three motors and the tail servo. The front rotors provide differential roll and collective lift, while the tail rotor magnitude and tilt angle are resolved from the vector components:

$$f_1 = \frac{1}{2}\left((f - f_{3,vert}) + \frac{M_1}{d_y}\right) \tag{20}$$

$$f_2 = \frac{1}{2}\left((f - f_{3,vert}) - \frac{M_1}{d_y}\right) \tag{21}$$

$$f_3 = \sqrt{f_{3,vert}^2 + f_{3,lat}^2} \tag{22}$$

$$\delta = \text{atan2}(f_{3,lat}, f_{3,vert}) \tag{23}$$

While this scheme ensures exact tracking of the desired virtual moment M and vertical thrust f, the generation of yaw torque necessitates a non-zero lateral component $f_{3,lat}$. This inherently produces a parasitic lateral force $\Delta = f_{3,lat}\vec{b}_2$ on the body, a coupling effect that is accounted for in the stability analysis.

IV. STABILITY ANALYSIS

A. Exponential Stability of Attitude Dynamics

The nonlinear control allocation scheme derived in Section II ensures that the control moment applied to the vehicle body is exactly the desired moment M. Consequently, the attitude dynamics are decoupled from the translational parasitic forces. We proceed with the proof of exponential stability on $SO(3)$ following the geometric framework established in [3].

Proposition 1. *Consider the attitude dynamics governed by* (7) *and the control moment* M *defined in* (18)*. Suppose the initial condition satisfies:*

$$\Psi(R(0), R_d(0)) < 2 \tag{24}$$

$$||e_\Omega(0)||^2 < \frac{2}{\lambda_{min}(J)} k_R (2 - \Psi(R(0), R_d(0))) \tag{25}$$

Then, the zero equilibrium of the tracking errors (e_R, e_Ω) *is exponentially stable.*

Proof. Let the Lyapunov function candidate $\mathcal{V}_R$ be defined as:

$$\mathcal{V}_R = \frac{1}{2} e_\Omega \cdot J e_\Omega + k_R \Psi(R, R_d) + c_2 e_R \cdot e_\Omega \tag{26}$$

where c_2 is a positive constant. To ensure $\mathcal{V}_R$ is positive definite, we choose c_2 sufficiently small such that:

$$c_2 < \min\left\{\sqrt{k_R \lambda_{min}(J)}, \frac{4 k_\Omega \lambda_{min}(J)^2}{k_\Omega^2 \lambda_{max}(J) + 4 k_R \lambda_{min}(J)^2}\right\} \tag{27}$$

We first bound $\mathcal{V}_R$ within the sublevel set $L_2 = \{(R, R_d) \mid \Psi < 2\}$. Defining the state vector $z_R = [||e_R||, ||e_\Omega||]^T$, we can establish the following inequality:

$$z_R^T W_1 z_R \leq \mathcal{V}_R \leq z_R^T W_2 z_R \tag{28}$$

where the matrices W_1 and W_2 are given by:

$$W_1 = \frac{1}{2}\begin{bmatrix} k_R & -c_2 \\ -c_2 & \lambda_{min}(J) \end{bmatrix}, \quad W_2 = \frac{1}{2}\begin{bmatrix} \frac{4k_R}{2-\psi} & c_2 \\ c_2 & \lambda_{max}(J) \end{bmatrix} \tag{29}$$

where ψ is an upper bound on the initial attitude error.

Next, we evaluate the time derivative of $\mathcal{V}_R$. The derivative of the error function is $\dot{\Psi} = e_R \cdot e_\Omega$. The angular velocity error dynamics are:

$$J\dot{e}_\Omega = M - \Omega \times J\Omega - J(\hat{\Omega} R^T R_d \Omega_d - R^T R_d \dot{\Omega}_d) \tag{30}$$

Substituting the control law M from (18), this simplifies to $J\dot{e}_\Omega = -k_R e_R - k_\Omega e_\Omega$. Taking the time derivative of $\mathcal{V}_R$:

$$\begin{aligned} \dot{\mathcal{V}}_R &= e_\Omega \cdot J\dot{e}_\Omega + k_R \dot{\Psi} + c_2(\dot{e}_R \cdot e_\Omega + e_R \cdot \dot{e}_\Omega) \\ &= e_\Omega \cdot (-k_R e_R - k_\Omega e_\Omega) + k_R (e_R \cdot e_\Omega) \\ &\quad + c_2(\dot{e}_R \cdot e_\Omega + e_R \cdot J^{-1}(-k_R e_R - k_\Omega e_\Omega)) \end{aligned} \tag{31}$$

Canceling the $k_R(e_R \cdot e_\Omega)$ terms and utilizing the kinematic property $||\dot{e}_R|| \leq ||e_\Omega||$, we bound the derivative:

$$\dot{\mathcal{V}}_R \leq -(k_\Omega - c_2)||e_\Omega||^2 - \frac{c_2 k_R}{\lambda_{max}(J)}||e_R||^2 + c_2 k_\Omega ||e_R||||e_\Omega|| \tag{32}$$

This can be written in quadratic form $\dot{\mathcal{V}}_R \leq -z_R^T W_3 z_R$, where:

$$W_3 = \begin{bmatrix} \frac{c_2 k_R}{\lambda_{max}(J)} & -\frac{c_2 k_\Omega}{2} \\ -\frac{c_2 k_\Omega}{2} & k_\Omega - c_2 \end{bmatrix} \tag{33}$$

Under the condition that c_2 is chosen small enough, W_3 is positive definite. Let $\lambda_{min}(W_3)$ denote its minimum eigenvalue. We then have:

$$\dot{\mathcal{V}}_R \leq -\lambda_{min}(W_3)||z_R||^2 \tag{34}$$

Combining this with the upper bound from (28), we obtain:

$$\dot{\mathcal{V}}_R \leq -\frac{\lambda_{min}(W_3)}{\lambda_{max}(W_2)} \mathcal{V}_R \tag{35}$$

This differential inequality implies that $\mathcal{V}_R(t) \leq \mathcal{V}_R(0) e^{-\alpha t}$ with rate $\alpha = \frac{\lambda_{min}(W_3)}{\lambda_{max}(W_2)}$. Since $\mathcal{V}_R$ is bounded from below by $||z_R||^2$, the tracking errors converge exponentially to zero. □

Remark 1. *The validity of the ideal allocation assumption relies on the principle of timescale separation between*

the actuator dynamics and the rigid body dynamics. The tricopter's actuators—specifically the electronic speed controllers driving the rotors and the servo mechanism tilting the tail rotor—operate with a bandwidth significantly higher than that of the vehicle's rotational attitude dynamics.

Consequently, the actuators are assumed to reach their commanded setpoints instantaneously relative to the evolution of the vehicle's orientation states (R, Ω). This allows us to neglect the transient lag of the servo mechanism and motor spin-up in the Lyapunov stability analysis, treating the physical control moment generated by the allocation scheme as mathematically equivalent to the desired virtual moment M.

B. Uniformly Ultimately Bounded (UUB) Stability of Translational Dynamics

Unlike the attitude dynamics, the translational dynamics are subject to a coupling force. The generation of the yaw moment M_3 via the servo tilt requires a lateral thrust component $f_{3,lat}$, which manifests as a parasitic force Δ in the body frame. We treat this as a bounded disturbance and prove Uniformly Ultimately Bounded (UUB) stability, similer to [5].

Proposition 2. *Consider the translational dynamics* (5) *with the control thrust f defined in* (17)*. Assume the yaw command is bounded such that the parasitic force satisfies $||\Delta(t)|| \leq \delta_{max}$ for all t. Then, the position and velocity tracking errors (e_x, e_v) are Uniformly Ultimately Bounded.*

Proof. The error dynamics for the position and velocity are given by:

$$\dot{e}_x = e_v \tag{36}$$

$$m\dot{e}_v = mge_3 + RF_b - m\ddot{x}_d \tag{37}$$

Substituting the control law for f and identifying the parasitic force $R\Delta$, we have:

$$m\dot{e}_v = -k_x e_x - k_v e_v + R\Delta + \xi(R, R_d) \tag{38}$$

where ξ represents vanishing perturbation terms dependent on the attitude error e_R. As shown in Proposition 1, e_R vanishes exponentially; therefore, we analyze the stability with respect to the persistent non-vanishing disturbance Δ.

Consider the Lyapunov function candidate:

$$\mathcal{V}_x = \frac{1}{2}k_x||e_x||^2 + \frac{1}{2}m||e_v||^2 + c_1 e_x \cdot e_v \tag{39}$$

where c_1 is a positive constant. We choose c_1 sufficiently small to ensure $\mathcal{V}_x$ is positive definite:

$$c_1 < \min\left\{\sqrt{k_x m}, \frac{4mk_x k_v}{4mk_x + k_v^2}\right\} \tag{40}$$

We define the state vector $z_x = [||e_x||, ||e_v||]^T$. Similar to the attitude proof, we bound $\mathcal{V}_x$ by quadratic functions of the state:

$$z_x^T M_1 z_x \leq \mathcal{V}_x \leq z_x^T M_2 z_x \tag{41}$$

where the matrices M_1 and M_2 are defined as:

$$M_1 = \frac{1}{2}\begin{bmatrix} k_x & -c_1 \\ -c_1 & m \end{bmatrix}, \quad M_2 = \frac{1}{2}\begin{bmatrix} k_x + c_1 & c_1 \\ c_1 & m \end{bmatrix} \tag{42}$$

Taking the time derivative of $\mathcal{V}_x$:

$$\begin{aligned}\dot{\mathcal{V}}_x &= k_x e_x \cdot e_v + e_v \cdot (-k_x e_x - k_v e_v + R\Delta) \\ &\quad + c_1\left(||e_v||^2 + e_x \cdot \frac{1}{m}(-k_x e_x - k_v e_v + R\Delta)\right)\end{aligned} \tag{43}$$

Simplifying and grouping the quadratic terms:

$$\begin{aligned}\dot{\mathcal{V}}_x &= -(k_v - c_1)||e_v||^2 - \frac{c_1 k_x}{m}||e_x||^2 - \frac{c_1 k_v}{m}e_x \cdot e_v \\ &\quad + \left(e_v + \frac{c_1}{m}e_x\right) \cdot R\Delta\end{aligned} \tag{44}$$

We can bound this expression using the state vector z_x:

$$\dot{\mathcal{V}}_x \leq -z_x^T M_3 z_x + \delta_{max}\left\|e_v + \frac{c_1}{m}e_x\right\| \tag{45}$$

where M_3 is given by:

$$M_3 = \begin{bmatrix} \frac{c_1 k_x}{m} & \frac{c_1 k_v}{2m} \\ \frac{c_1 k_v}{2m} & k_v - c_1 \end{bmatrix} \tag{46}$$

Using the inequality $||e_v + \frac{c_1}{m}e_x|| \leq ||e_v|| + \frac{c_1}{m}||e_x|| \leq \max\{1, \frac{c_1}{m}\}||z_x||$, we obtain:

$$\dot{\mathcal{V}}_x \leq -\lambda_{min}(M_3)||z_x||^2 + \delta_{max}\theta||z_x|| \tag{47}$$

where $\theta = \sqrt{1 + (c_1/m)^2}$. For $\dot{\mathcal{V}}_x$ to be negative definite, the quadratic stabilizing term must dominate the linear disturbance. This occurs when:

$$||z_x|| > \frac{\delta_{max}\theta}{\theta_{min}(1 - \alpha)} \triangleq \mu \tag{48}$$

where $0 < \alpha < 1$. This implies that the states converge exponentially to the ultimate bound ball $\mathcal{B}_\mu = \{z_x \in \mathbb{R}^2 \mid ||z_x|| \leq \mu\}$. Specifically, the squared norm of the error satisfies:

$$\limsup_{t\to\infty}||z_x(t)||^2 \leq \frac{\lambda_{max}(M_2)}{\lambda_{min}(M_1)}\left(\frac{\delta_{max}\theta}{\lambda_{min}(M_3)}\right)^2 \tag{49}$$

Thus, the system is Uniformly Ultimately Bounded. □

C. Almost Global Attractiveness to the Ultimate Bound

Proposition 2 requires that the initial attitude error is less than $90°$ ($\Psi < 1$) to ensure the thrust vector component opposing gravity dominates the dynamics. Suppose this is not satisfied, i.e., $1 \leq \Psi(R(0), R_d(0)) < 2$.

From Proposition 1, we are guaranteed that the attitude error function Ψ decreases exponentially regardless of the translational state. Therefore, the system will enter the region of attraction of Proposition 2 in finite time. By combining the exponential stability of the attitude dynamics with the UUB stability of the translational dynamics, we establish almost global attractiveness to the ultimate bound.

Proposition 3 (Almost Global Attractiveness)**.** *Consider the control system designed according to Propositions 1 and 2. Suppose the initial condition satisfies:*

$$1 \leq \Psi(R(0), R_d(0)) < 2 \tag{50}$$

$$||e_\Omega(0)||^2 < \frac{2}{\lambda_{min}(J)} k_R (2 - \Psi(R(0), R_d(0))) \tag{51}$$

Then, the state trajectory of the complete dynamics converges to the ultimate bound $\mathcal{B}_\mu$ defined in Proposition 2.

Proof. From Proposition 1, the attitude error $\Psi(t)$ decays exponentially. Thus, for any initial condition satisfying (38), there exists a finite time $t^* > 0$ such that $\Psi(t^*) < 1$.

During the finite interval $t \in [0, t^*)$, the attitude error may be large. However, since the total thrust f and external forces (gravity) are bounded, the time rate of change of the translational states $\dot{e}_v$ is bounded. Consequently, the position and velocity errors (e_x, e_v) can only grow by a finite amount during this interval and remain bounded.

For all $t \geq t^*$, the condition $\Psi(t) < 1$ is satisfied, and the system enters the region of attraction established in Proposition 2. From this time forward, the bounded drift accumulated during the interval $[0, t^*)$ is exponentially suppressed, and the errors (e_x, e_v) converge to the ultimate bound $\mathcal{B}_\mu$. Since the initial region of attraction for the attitude dynamics covers $SO(3)$ almost globally (excluding only the set of states where the attitude error is exactly $180°$), the ultimate bound $\mathcal{B}_\mu$ is almost globally attractive. □

Remark 2 (Thrust Modulation)**.** *A critical feature enabling this global recovery is the geometric definition of the thrust input f in* (17)*. The dot product with Re_3 acts as a geometric dimmer switch. When the vehicle attitude has a large error (e.g., $\Psi \approx 1$ or $90°$ tilt), the projection of the desired force onto the body axis is small, naturally reducing the applied thrust f. This prevents the vehicle from inadvertently accelerating in the wrong direction while the attitude controller works to restore the orientation.*

D. Properties and Extensions

One of the unique properties of the presented controller is that it is directly developed on $SE(3)$ using rotation matrices. Therefore, it avoids the complexities and singularities associated with local coordinates of $SO(3)$, such as Euler angles. It also avoids the ambiguities that arise when using quaternions to represent the attitude dynamics. As the three-sphere S^3 double covers $SO(3)$, any attitude feedback controller designed in terms of quaternions could yield different control inputs depending on the choice of quaternion vectors, potentially leading to unwinding phenomena, where the controller forces the vehicle to perform a full $360°$ rotation to reach the target rather than taking the shorter geodesic path. In this paper, the use of rotation matrices in the controller design and stability analysis completely eliminates these difficulties.

A distinct feature of this work, compared to the quadrotor case, is the explicit handling of actuator coupling through the nonlinear allocation scheme. While the quadrotor relies on a fixed linear mapping, the tricopter requires a continuous re-configuration of the rear servo angle δ and thrust f_3 to realize the desired virtual controls. Our proposed allocation method provides an exact analytical solution to this nonlinear problem, ensuring that the attitude dynamics are decoupled from the translational actuation limits, while isolating the coupling effects to the translational dynamics as a bounded disturbance.

This separation allows for a nuanced stability result: the attitude dynamics exhibit exponential stability, while the translational dynamics exhibit Uniformly Ultimately Bounded (UUB) stability. This theoretical result aligns with the physical intuition of tricopter flight: the vehicle can point its heading with arbitrary precision, but aggressive yaw maneuvers will inevitably induce small, transient lateral drifts due to the vectoring thrust component. The UUB radius quantifies this drift, providing a rigorous metric for the tightness of the translational tracking during complex maneuvers.

In Propositions 1 and 3, exponential stability and attractiveness to the ultimate bound are guaranteed for almost all initial attitude errors. The attitude error function defined in (12) has critical points in the identity matrix (the global minimum) and in the rotations that represent a deviation $180°$ (unstable equilibria). Only these non-identity critical points, which constitute a set of measure zero (a two-dimensional subspace of the three-dimensional $SO(3)$), lie outside the region of attraction. Thus, we claim almost global stability properties.

It is worth noting that the proposed geometric controller is analogous to a Proportional-Derivative (PD) controller on the manifold. While it guarantees exponential stability for the nominal model, it lacks integral action to compensate for persistent, unstructured disturbances such as center-of-mass shifts or steady wind fields. Consequently, in the presence of such perturbations, the system may exhibit steady-state tracking errors. Future work could incorporate geometric integral feedback terms to robustly reject such persistent disturbances and eliminate these offsets.

This controller can be extended to address actuator saturation. In the current formulation, we assume the servo angle δ and motor thrusts f_i are unbounded. In practice, the servo has a finite range (typically $\pm 90°$) and motors have maximum thrust limits. The geometric framework allows for the integration of saturation functions into the virtual control definition, or the modification of the reference trajectory $x_d(t)$ to ensure the required inputs remain within the feasible polytope of the tricopter's actuation space.

V. SIMULATION RESULTS

To validate the proposed geometric control framework and the stability properties derived in Section IV, we developed a numerical simulation environment. The simulation models the full nonlinear dynamics of the tricopter on $SE(3)$, including actuator saturation and the nonlinear control allocation map derived in Section II.

A. System Configuration and Parameter Identification

The simulation parameters were selected to represent a standard medium-sized tricopter frame in a Y-configuration. The total mass of the vehicle is $m = 1.0$ kg. The geometric arm lengths were defined as $d_x = d_y = 0.4$ m for the front rotors and $d_t = 0.5$ m for the rear tail rotor.

As the exact rotational inertia matrix J is difficult to measure without an experimental setup, we derived a physical approximation by modeling the motors as point masses distributed at the arm extremities. Assuming a motor mass $m_{arm} \approx 0.2$ kg, the diagonal inertia components were calculated as:

$$J_{xx} \approx 2m_{arm}d_y^2 = 0.064\,\text{kg}\cdot\text{m}^2 \tag{52}$$

$$J_{yy} \approx 2m_{arm}d_x^2 + m_{arm}d_t^2 = 0.114\,\text{kg}\cdot\text{m}^2 \tag{53}$$

$$J_{zz} \approx J_{xx} + J_{yy} = 0.178\,\text{kg}\cdot\text{m}^2 \tag{54}$$

This results in an inertia matrix $J = \text{diag}(0.064, 0.114, 0.178)$. Notably, the tricopter exhibits significant asymmetry ($J_{yy} \approx 1.8J_{xx}$), which necessitates the use of a matrix-based attitude gain structure rather than scalar gains to ensure uniform damping across axes.

B. Controller Tuning via Pole Placement

The control gains were derived using a pole-placement strategy based on the principle of timescale separation. To satisfy the assumptions of the stability proof, the inner attitude loop was tuned to be significantly faster than the outer translational loop.

1) Translational Gains: The translational error dynamics were modeled as a second-order linear system. We selected a natural frequency $\omega_{n,pos} = 2.0$ rad/s and a critical damping ratio $\zeta_{pos} = 1.0$ to ensure a settling time of approximately 2.0 seconds with no overshoot. The resulting gains are:

$$k_x = m\omega_{n,pos}^2 = 4.0, \quad k_v = 2m\zeta_{pos}\omega_{n,pos} = 4.0 \tag{55}$$

2) Attitude Gains: The rotational dynamics were tuned to be five times faster than the translational dynamics ($\omega_{n,rot} = 10.0$ rad/s) to ensure the vehicle orientation tracks the desired thrust vector b_{3d} nearly instantaneously. We selected a damping ratio $\zeta_{rot} = 0.9$ to provide robust performance. The gain matrices K_R and K_Ω were scaled by the maximum principle moment of inertia $\lambda_{max}(J) \approx 0.178$:

$$K_R = \lambda_{max}(J)\omega_{n,rot}^2 I_{3\times3} \approx 17.8I_{3\times3} \tag{56}$$

$$K_\Omega = \lambda_{max}(J)2\zeta_{rot}\omega_{n,rot}I_{3\times3} \approx 3.2I_{3\times3} \tag{57}$$

We verified that these gains satisfy the stability condition required by Proposition 1: $k_\Omega^2 > 4k_R\lambda_{min}(J)^2/\lambda_{max}(J)$.

C. Actuator Constraints and Inverted Flight Logic

The simulation incorporates physical actuator limits, specifically clamping the tail servo angle δ to $\pm 90^\circ$ and enforcing non-negative motor thrusts $f_i \geq 0$.

A critical modification was required for the control allocation during inverted flight phases. When the vehicle is upside down ($\Psi > 1 = 90^\circ$), the geometric controller requests a negative total thrust $f < 0$ to accelerate downward (relative to the body). If passed directly to the allocation solver with non-negative constraints, this results in all motors commanding zero thrust, leading to a total loss of control authority.

To resolve this, we implemented a priority logic within the allocation scheme. When $f_{des} < 0$, the thrust target is clamped to zero, but the moment targets M_{des} are preserved. This forces the solver to generate differential thrust (e.g., $f_1 > 0, f_2 = 0$) to satisfy the torque request, allowing the vehicle to right itself even during free-fall.

D. Performance Scenarios

We evaluated the controller in two distinct scenarios:

1) Normal Trajectory Tracking: The vehicle was commanded to follow a diagonal trajectory from the origin to $x_d = [1, 1, -1]^T$. As shown in figure 1, the controller demonstrated smooth convergence with zero steady-state error.

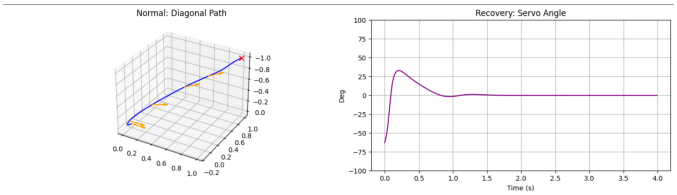

Fig. 2. UAV maneuver from an initial position of [0,0,0] to [1,1,-1]. The first plot illustrates the drone's path and orientation through space. The second plot shows the tail servo actuation throughout the maneuver.

2) Upside-Down Recovery: To demonstrate the almost global stability properties, the vehicle was initialized with an initial roll angle of 178° (nearly inverted). As shown in Fig. 3, the controller successfully recovers from the roll and stabilizes its altitude.

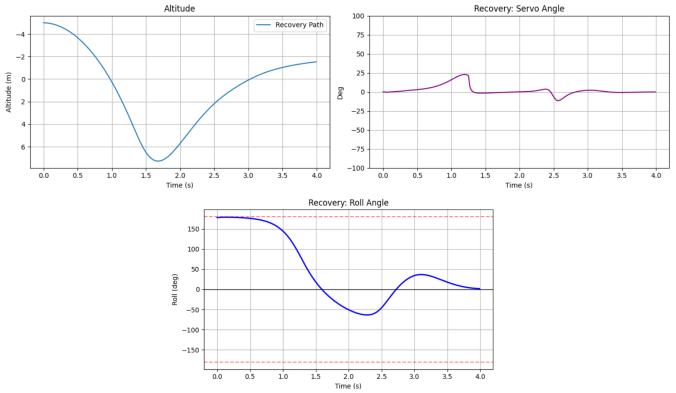

Fig. 3. Simulation of recovery maneuver from an initial 178° roll angle. The first plot illustrates the altitude the drone follows during the maneuver. The second plot shows the tail servo actuation throughout the maneuver. The third image shows the drone's roll throughout the maneuver.

REFERENCES

[1] F. Bullo and A. D. Lewis, *Geometric control of mechanical systems: modeling, analysis, and design for simple mechanical control systems*. Springer Science & Business Media, 2005, vol. 49.

[2] T. Lee, N. H. McClamroch, and M. Leok, "A lie group variational integrator for the attitude dynamics of a rigid body with applications to the 3d pendulum," in *Proceedings of 2005 IEEE Conference on Control Applications*. IEEE, 2005, pp. 962–967.

[3] T. Lee, M. Leok, and N. H. McClamroch, "Geometric tracking control of a quadrotor uav on se(3)," in *49th IEEE Conference on Decision and Control (CDC)*. IEEE, 2010, pp. 5420–5425.

[4] F. Goodarzi, D. Lee, and T. Lee, "Geometric nonlinear pid control of a quadrotor uav on se(3)," in *2013 European Control Conference (ECC)*. IEEE, 2013, pp. 3845–3850.

[5] M. Ramp and E. Papadopoulos, "On modeling and control of a holonomic vectoring tricopter," in *2015 IEEE/RSJ International Conference on Intelligent Robots and Systems (IROS)*. IEEE, 2015, pp. 662–668.